Summer 2024

Theoretical Modeling And Experimental Investigation Of Phase Selection During Rapid Solidification Of Alloys

Azeez Aremu Akinbo
Missouri University of Science and Technology

Department:

THEORETICAL MODELING AND EXPERIMENTAL INVESTIGATION OF PHASE SELECTION DURING RAPID SOLIDIFICATION OF ALLOYS

by

AZEEZ AREMU AKINBO

A THESIS

Presented to the Graduate Faculty of the

MISSOURI UNIVERSITY OF SCIENCE AND TECHNOLOGY

In Partial Fulfillment of the Requirements for the Degree

MASTER OF SCIENCE

in

MATERIALS SCIENCE AND ENGINEERING

2024

Approved by:

Yijia Gu, Advisor
Joseph Newkirk
Mario Buchely

PUBLICATION THESIS OPTION

This thesis consists of the following article, formatted in the style used by the Missouri University of Science and Technology:

Paper I, found on pages 12-38, has been submitted for publication by Azeez, Akinbo & Yijia Gu (2023). Modeling of Phase Selection and Extended Solubility in Rapidly Solidified Alloys.

ABSTRACT

A novel model, rooted in time-dependent nucleation theory, has been created to explore how rapid solidification affects the extended solubility in metal alloys. This model was used to forecast solubility concerning undercooling in multiple binary aluminum (Al) alloys, and its predictions for both eutectic and peritectic systems closely match experimental data. It was demonstrated that this developed model surpasses the T0 line method, which does not consider the kinetic aspects of nucleation. Furthermore, the model can be extended to ternary and multicomponent phases by assuming that the scarcest element or the slowest diffusing component restricts nucleation. Al-Cu and Al-Cr, vital for aerospace and automobile applications, were investigated experimentally. Fiber Bragg Grating Sensors (FBGs) and K-type thermocouples were used to study the solidification characteristics of the alloys by measuring cooling rates at various positions in the cavity of a copper wedge mold. The result could be more consistent and reliable but can be improved upon in the future for further study. This new model's practicality and dependability make it a valuable tool for innovating alloy design in rapid solidification processes, such as additive manufacturing.

ACKNOWLEDGMENTS

I would also like to express my profound appreciation to my supervisor, Dr. Yijia Gu. Your constant encouragement, unwavering support, and motivational guidance have shaped my academic growth. Your belief in my abilities has empowered me to overcome obstacles and strive for excellence in my research pursuits. Your mentorship has been invaluable, and I am truly fortunate to have worked under your guidance.

I want to thank the exceptional staff and faculty in the Department of Materials Science and Engineering. I am deeply thankful for the unwavering support and assistance from Teneke, Emily, Brian, and Nathan staff members. Moreover, I express my profound gratitude to Dr. Newkirk and his research group for their constant support and guidance on the metallography of my specimens. I am incredibly grateful for Dr Mario Buchely's unwavering support and guidance towards my experimental setup and trials.

I would love to thank my family for their unconditional love, unwavering support, and prayers throughout my academic journey. I am incredibly grateful to my uncle for his fatherly support and financial assistance in obtaining a scholarship to pursue my studies in the USA. I thank my friends and colleagues for your encouragement and unwavering support. Your belief in my potential has been a constant source of motivation.

Lastly, I am immensely thankful to Nadege and Mazeedah for always being there for me in times of need. Your comfort, love, and encouragement have lifted me when I fell on my research and driven me to do more. I thank myself for not giving up on myself.

TABLE OF CONTENTS

Page

LIST OF ILLUSTRATIONS

LIST OF TABLES

PAPER I Page

1. INTRODUCTION

For the past few years, additive manufacturing (AM), which involves joining materials to make parts or objects from 3D model data, usually in a layer-by-layer fashion, has contributed immensely to the success of the manufacturing industry. AM processes produce a near-net-shape component used in various sectors with controlled microstructure and properties. Fusion-based metal AM processes such as powder bed fusion utilize a rapid solidification process to enhance the development of new microstructure, with refined grain structures, extended solubility, and reduced partition of solute[1]. Rapid solidification is a non-equilibrium process widely known to increase solid solubility and the formation of nanocrystalline materials, metastable phases, quasi-crystalline phases, and bulk metallic glasses. How the microstructures evolve as a function of the solidification velocity has been a subject of intense investigation over the past few years. Specifically, the prediction of the phase selection during this process needs to be more conclusive. Rapid solidification processes such as melt spinning, liquid metal atomization, electromagnetic levitation, etc., also face the challenges of understanding the phase selection of various materials[2].

Additively manufactured parts undergo a rapid solidification process, which involves the quick extraction of heat ranging from 100 K/s to 106 K/s from the molten melt because of different energy sources such as laser [1]. Rapid solidification (RS) processes are known for producing materials with metastable and refined microstructures and improved properties. In RS, the constitutional change is highly system-specific and is associated with significant departures from equilibrium due to the large undercoolings

applicable at the rapidly advancing solidification front. The microstructural refinement is less system-specific and results from the short diffusion distances associated with the rapidly advancing solidification front [2][3]. Constitutional effects of rapid solidification include the extension of solid solubility and the formation of metastable phases due to nucleation and growth competition between the candidate phases, whether equilibrium or not, in the undercooled melt [1][4]. The effect includes extended solubilities of alloying elements in alloys, increased chemical homogeneity, and produce metastable phases [6][7]. For example, the solubility of scandium in aluminum increases from 0.01wt% to 0.23wt% after solidification[3], [4].

RS of aluminum alloys has been reported to increase the mechanical properties of aluminum alloys through solid solution strengthening because of the alloying element going into solid solution with the α-Al. Aluminum alloys have been studied for decades. They are an excellent choice in the aerospace and automobile industries due to their various mechanical properties, such as lightweight, high strength, low density, etc. However, improving the stability of aluminum alloys for use at above 425ºC (0.75Tm) is a primary concern and has been studied for decades [8]. It is known that over the last decades, there has been an increasing demand for lightweight materials from multiple industrial applications. Due to low solubility in aluminum, elements such as scandium with a concentration of 0.01wt% during solidification fill the crystal lattice to form an interstitial solid solution α-Al and thereby increase the strength of Al-Sc to around 400Mpa to 500Mpa. Alloying elements, such as Mg, Mn, Fe, Si, and so on, are known to form a solid solution that strengthens with aluminum during rapid solidification. Various compositions of main alloying elements were investigated, and Mn was reported to have

the highest tensile strength of approximately 500Mpa and retain elongation as compared to Mg, which has around 410Mpa [9]. The strengthening effect was predicted due to the interaction between Mn atoms and trace elements such as Si in a solid solution [10]. Due to the low solubility and diffusivity exhibited by those alloying elements, their strengthening effects are limited. Hence, it is essential to understand the phase selection and know the maximum solubility of the alloy during RS for designing materials with enhanced properties.

Solid solubility in metallurgy is the extent to which an alloying element dissolves completely in an element's matrix without forming another new phase. The solid solubility of an alloy is essential and contributes to the solid solution-strengthening mechanism of an alloy. Precipitation strengthening or age hardening involves the ability of a material to withstand elevated temperatures. It is dependent on the solid solubility of the alloy to be able to form a precipitate with a refined grain structure that will withstand coarsening and dislocation of motion [3]. We must understand the phase selection for extended solubility and microstructure development during rapid solidification. The high cooling rate is known to increase the solid solubility of an alloy. The solute atoms can be suppressed due to large undercooling; hence, the matrix phase will be the only phase formed during solidification. The solute atoms may be trapped in the matrix phase during this process, and the solubility of an alloy will increase.

Several authors have published papers on different theories and models to study the phase selection and extended solubility of rapidly solidified alloys[5], [6], [7]. Shao et al. developed a phase selection model based on the time-dependent nucleation theory[2]. The model introduced incubation time τ, the transient period before the nuclei reach their

steady state[8]. However, their studies suffer some setbacks, such as the outdated entropy of fusion and difficulty in calculating diffusivity, which makes the model incapable of correctly predicting the phase selection and the extended solubility. Extended solubility was also modeled by[4] using the T_0 concept. The T_0 temperature curve corresponds to the temperature where the free energies of an alloy's liquid and solid phases are the same. The curve corresponds to the maximum thermodynamical solubility possible for an alloy's composition.

The research aims to develop a new mathematical model to predict rapidly solidified alloys' phase selection and extended solubility. Ingot casting using a copper mold was performed to validate our model and study the microstructure of the phases resulting from the rapid solidification process.

The thesis consists of four sections. Section 1 presents the Introduction, which includes the background of the study, knowledge gap, problem statement, and scope of the study. Section 2, the literature review, reviews past studies such as modeling using Time-dependent nucleation theory (TDNT) and T_0 curve. The chapter discusses experimental procedures such as using the wedge mold to capture different cooling rates at other positions, which can be used to validate modeling of rapidly solidified alloys, etc. The section also contains a research paper titled “Modeling of Phase Selection and Extended Solubility in Rapidly Solidified Alloys,” which was accepted and published by the Journal of Metallurgical and Materials Transactions A. Section 3 consists of the experimental procedures, results, and discussion of the aluminum alloys (Al-4.5wt%Cu and Al-1wt%Cr) used in the study. Section 4 consists of the conclusion and recommendations for future research.

2. LITERATURE REVIEW

This section reviews the different theoretical models that can be utilized to study the prediction of phase selection and experimental investigation. The nucleation model using the Time-Dependent Nucleation Theory and the T0 curve are explained in detail. In addition, the experimental method using a copper wedge mold to obtain a temperature value to obtain a cooling rate is reviewed, which can be used to investigate extended solubilities of different alloying elements in the matrix compound.

2.1. PHASE SELECTION AND NUCLEATION

Nucleation involves the appearance of small particles, or nuclei of the new phase (often consisting of only a few hundred atoms), which can grow. During the growth stage, these nuclei increase in size, which results in the disappearance of some (or all) of the parent phase. The transformation reaches completion if the growth of these new-phase particles is allowed to proceed until the equilibrium fraction is attained. There are two types of nucleation: homogeneous and heterogeneous.[2] The distinction between them is made according to the site at which nucleating events occur. For the homogeneous type, nuclei of the new phase form uniformly throughout the parent phase, whereas for the heterogeneous type, nuclei form preferentially at structural inhomogeneities, such as container surfaces, insoluble impurities, grain boundaries, and dislocations. Nucleation undercooling is of prime importance in determining the microstructure of the RS product. Calculations based on steady-state classical nucleation

theory have suggested that phase selection is determined by nucleation, especially at large melt undercoolings [3, 4].

Interpretations of nucleation experiments and formulations of most nucleation theories, including those used in alloy design, often assume a constant nucleation rate. While frequently true, this assumption needs to be corrected in many cases. For example, time-dependent nucleation theory is essential in many first-order phase changes, including vapor condensation, liquid phase separation, crystallization of undercooled liquids, glass formation, and devitrification of glasses. The problem of nucleation in undercooled melts is still unresolved regarding the operating nucleation mechanisms and the role of different types of nucleates in phase selection and subsequent growth and solidification.

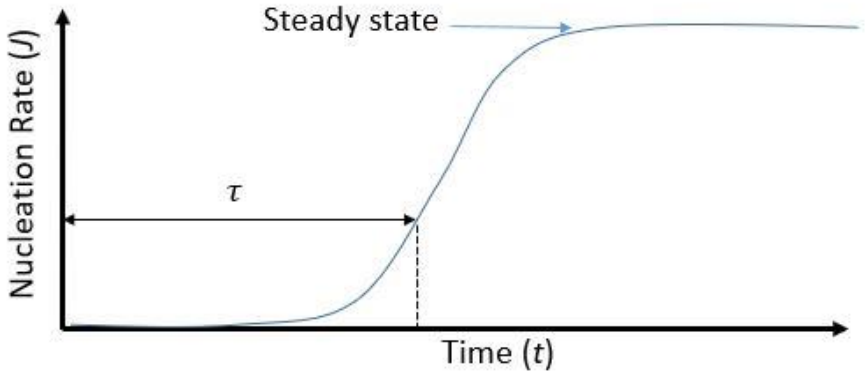

Figure 2.1: Steady-state and incubation time for thermal nucleation.

Many researchers have tried different theories and models to predict phase selection and the extent of solubility. The steady-state nucleation theory treatment is adequate during solidification, provided the cluster population evolves sufficiently

rapidly as the temperature changes. This may only be sometimes true during solidification at significant cooling rates, as shown for some glass-forming systems. As shown in Figure 2.1 above, the nucleation rate J is nearly zero when $t < \tau$, and only when t reaches τ, the incubation time, can nucleation start with a rate Js. Shaos et al. were one of the few papers using Time-Dependent Nucleation Theory (TDNT) to predict the competing phases of aluminum alloys such as Al-Cr, Al-Ti, and Al-Zr, respectively [3]. However, thermodynamic properties such as entropy of fusion used during the evaluation of undercooling are outdated, and the viscosity coefficient is hard to obtain, resulting in errors in their model. (The current thermodynamic database shows improved accuracy due to a large number of experiment data.) Investigation on the phase selection and extended solid solubility of the ternary and quaternary systems with little or no data are available yet [7].

2.2. MODELING EXTENDED SOLUBILITY USING T_0

The extended solubility of several eutectic systems of aluminum alloys such as Al-Si, Al-Fe, and Al-Mg was modeled using the so-called T_0 curve [4]. The T_0 concept was used to extrapolate the liquidus and solidus lines to be able to calculate the T_0 curve for lower temperature below the eutectic temperature. The T_0 curve is the locus of compositions and temperatures at which the free Gibbs energy of the liquid and solid phases is equal. Hence, the maximum solid solubility thermodynamically possible for a given composition at a given temperature can be determined if the Gibbs free energy of both phases is known. This method does not work for the peritectic system, as the T_0 curve lies on the left side of the solidus (lower solute concentration). The peritectic

system is different because the alloying element's low solid solubility in aluminum means the maximum solubility is always better than the peritectic reaction composition. However, the T_0 curve can only be obtained analytically using a thermodynamics database.

Several scholars worked together to formulate equations for different ranges of temperatures for other alloys. Their equations can be utilized and solved analytically to calculate the T_0 curve[9]. Figure 2.2 shows a typical phase diagram with phase composition at Co, liquidus temperature line T_L, solidus line Ts, and T_0 line, respectively. The shaded portion of the phase diagram shows the range of possible solid compositions that can form from a liquid of composition C0 at various temperatures.

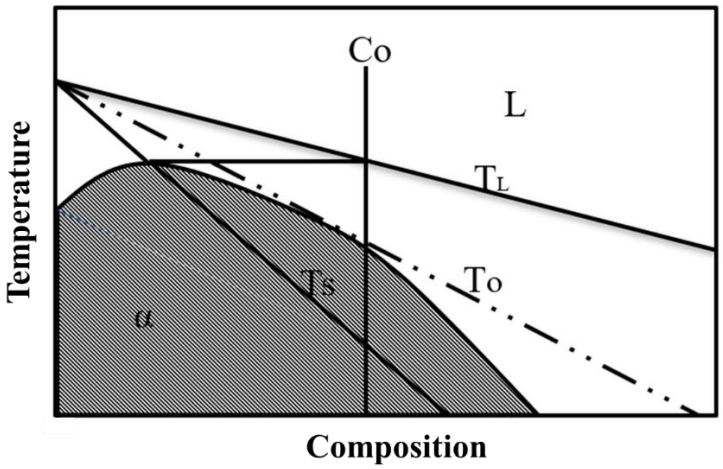

Figure 2.2: The thermodynamically allowed maximum solid solubility during solidification at composition Co.

2.3. RAPID SOLIDIFICATION EXPERIMENT USING A WEDGE MOLD

Ichikawa et al. investigated the effect of cooling rate on aluminum alloys (Al-Cr, Al-Mn, Al-Zr) during rapid solidification. They deduced that the square of undercooling

is proportional to the cooling rate of different alloys, and the undercooling degree increases with increasing alloying elements [10]. The experimental setup using thermocouple design efficiently alloys with desired improved properties are shown in figure (3) below[11]. The aluminum alloys were melted in a furnace at around 850ºC to dissolve all the intermetallic phases thoroughly and then poured into the copper wedge mold with the mold wall covered with ice water at 0ºC for rapid solidification. A thermocouple was inserted into the mold, and an oscilloscope was used to record the temperature change, solidification time during solidification, and the data used to calculate the cooling rate of different alloy compositions.

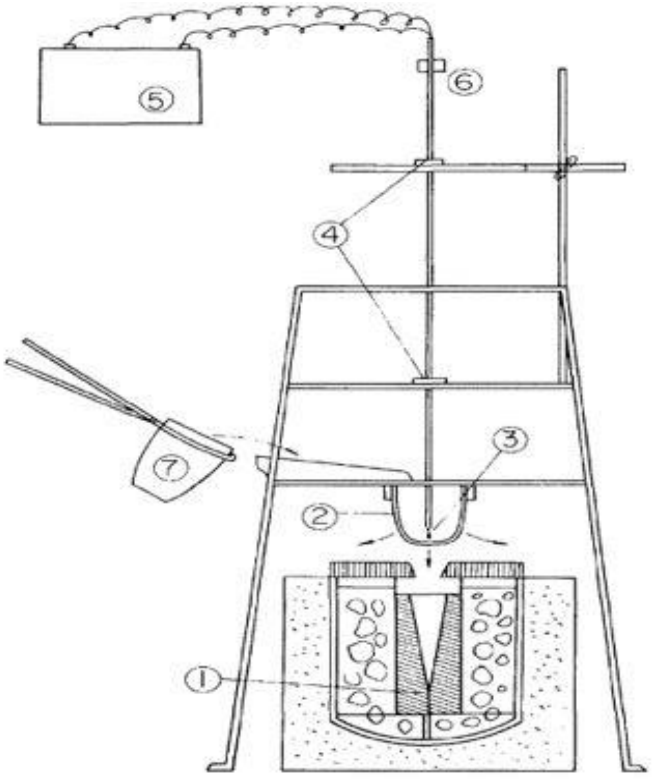

Figure 2.3: Schematic of copper mold and apparatus for casting and cooling rate[12].

The experiment setup includes:

1. Wedge-type mold, holding at 0ºC;
2. Crucible;
3. Thermo-couple;
4. Guide;
5. Recorder;
6. Controller for dropping thermos-couple;
7. Crucible used for melting and as ladle.

2.4. RESEARCH IMPACTS

a) Novel Alloys: The capability to understand the phases that can be developed during non-equilibrium rapid solidification enhances the ability to design novel materials for specific applications such as aerospace, automobile, and other engineering industries. Extending the solid solubility and being able to calculate the maximum solid solubility of an alloy enhance industries to be able to produce materials with specific mechanical properties depending on the application[9][4]. Aluminum can be alloyed with elements such as Zr and Ti to improve the overall creep resistance, which would make it more readily available for elevated temperature applications (above 300°C), a limitation of the current aluminum alloys [3]. The research outcome will make aluminum alloy selection a favorable material due to its high strength-to-weight ratio. Understanding solubility in aluminum during Additive manufacturing processes can produce attractive fusion-based metal AM with unique properties and microstructure.

b) Recycling and tolerance of impurities: Recycling can improve public welfare with lower emissions than new material processing. Improving the recyclability reduces the amount of new aluminum manufactured from bauxite. Producing aluminum from bauxite requires massive amounts of energy and mines to supply the bauxite. Mines cause erosion, carbon emissions, and habitat loss to local areas. Refining processes can contaminate water and air around a production site[13]. Reducing the demand for this process can improve public welfare and health. Aluminum is already a very recyclable material, which is advantageous because it saves energy costs and reduces potentially harmful waste to the environment. By understanding the extended solubility of various elements in aluminum, engineers can recycle even more aluminum without removing impurity elements. Also, improving the solid solution strengthening of aluminum alloys allows them to move into higher-strength applications where less recyclable materials are dominant. The application of aluminum alloys in the industry can also save energy costs, such as improving the fuel efficiency of vehicles since it is a lighter-weight material.

PAPER

I. MODELING PHASE SELECTION AND EXTENDED SOLUBILITY IN RAPID SOLIDIFIED ALLOYS

Azeez Akinbo, and Yijia Gu*

Department of Material Science and Engineering, Missouri University of Science and Technology, Rolla, Missouri, 65409, USA

*Corresponding Author: yijia.gu@mst.edu

ABSTRACT

A new phase selection model based on the time-dependent nucleation theory was developed to investigate the effect of rapid solidification on extended solubility. The model was applied to predict the solubility as a function of undercooling for several binary Al alloys. The predictions of both eutectic and peritectic systems show good agreement with experimental data. It was demonstrated that the developed model is better than the T_0 line method, which neglected the kinetic process of nucleation. Furthermore, the model can also be applied to ternary and multicomponent phases assuming the nucleation is limited by the scarcest species or the slowest diffuser. The feasibility and reliability of the new model make it a useful tool for novel alloy design for rapid solidification processes such as additive manufacturing.

1. INTRODUCTION

In recent years, the manufacturing community has witnessed a blossom in the research field of 3D printing or additive manufacturing (AM). AM integrates the microscopical material structure synthesis and macroscopic component shaping into one single operation, which promises the direct production of a near-net-shape component with controlled microstructures and properties. In addition, the fusion-based metal AM, which exploited the non-equilibrium process of rapid solidification, enables the development of novel microstructures with extended solubility, reduced partitioning of solute, and refined structures[14], and opens up a new horizon of microstructure synthesis to achieve exotic properties in alloys. However, due to the large undercooling at the rapidly advancing solidification front, the phase selection in rapid solidification deviates from the equilibrium phase diagram, imposing a significant challenge in the understanding of microstructure development during AM. Even in other well-studied rapid solidification processes, such as liquid metal atomization and melt spinning, understanding the phase selection is still challenging[15].

One major benefit of the deviated phase selection due to the rapid solidification is the extended solubility. Solid solubility describes the extent of an alloying element dissolved in the matrix solid solution phase without forming another solid phase. It is an important property for alloy development, as it is related to the two major strengthening mechanisms. First, it defines the ceiling of solid solution strengthening. Second, it determines the potential of precipitation strengthening or age hardening, which is one of the most effective strengthening mechanisms for non-ferrous alloys. The maximum solid

solubility is found to increase with the cooling rate as well as the undercooling. If all the other solid phases are suppressed by rapid solidification, the matrix phase will become the first to solidify. Thus, the solute atoms that may form other primary solid phases during equilibrium solidification will stay in the matrix phase, and hence the solid solubility of the alloying element is increased. Therefore, rapid solidification processes, including levitation, atomization, melt spinning, and AM, have the potential to extend the maximum solid solubility and fabricate components with unprecedented properties. However, the experimental data on supersaturation is limited to a few alloy systems, and only the maximum solubility is listed[16], [17]. Furthermore, the extended solubility is not a fixed value but a function of interface temperature (or undercooling), and it is also affected by the interface velocity[15]. On the experimental side, systematic studies on the dependence of extended solubility on undercooling are very scarce[15], [18], as most recent rapid solidification studies focused on the microstructure formation or phase selection for a given solidification condition (one single undercooling or cooling rate), including levitation[19], [20], [21], [22], [23], [24], [25], [26], atomization[27], melt spinning[28], [29], [30], and AM[31], [32], [33], [34], [35], [36], [37], [38], [39]. Theoretical models of extended solubility are also very scarce, although much progress has been made regarding modeling rapid solidification processes[40], [41], [42]. In the following, we briefly discuss the existing models of extended solubility.

To predict the extension of solid solubility in rapid solidification, understanding the mechanism of phase selection is the key. There have been many attempts to model phase selection and extended solubility in the past few decades. The phase selection under non-equilibrium conditions was first modeled using the so-called T_0 line. The T_0

temperature is defined by the thermodynamic condition that for a given composition c, the free energy of the solid phase eq liquid, G^s (c,T_0)=G^l (c,T_0), as shown in Figure 1. Therefore, the T_0 line describes when the diffusionless solidification is thermodynamically allowed[43]. If the Gibbs free energies of the liquid and solid phases of an alloy are known, one can determine the maximum solid composition (maximum solid solubility) thermodynamically possible for a given composition at a given temperature[44]. This method determines the maximum possible solid solubility, which can be achieved by complete solute trapping at high enough interfacial velocity. However, this method does not work for pthe peritectic system since the cap T_0 line lies on the left side of the solidus illustrated in Figure 1(b). Later, based on the time-dependent nucleation theory (TDNT), Shao and Tsakiropoulos[45] developed a phase selection model for rapid solidification, which can be used to calculate the extended solubility for both eutectic and peritectic systems. This model was adopted to investigate phase selection and to explain experimental observations in recent AM studies such as selective laser melting (SLM) and electron beam melting (EBM) [31], [32], [33], [34], [35], [36], [37], [38], [39]. However, this model estimates the diffusivity using viscosity, which may introduce large uncertainty. Additionally, the entropy of fusion used in their work needs to be updated. Hence, this model has limited capability in predicting the extended solubility for a given composition and undercooling/cooling rate. In addition, how this model is related to the T_0 line method has yet to be studied, except we know that it is from kinetic theory and the other one is purely from thermodynamics.

In this work, we developed a new model based on Shao and Tsakiropoulos's TDNT model by eliminating the kinetic parameters. The new model can be used to

predict the phase selection and the associated extended solubility for a given undercooling for both eutectic and peritectic systems. The thermodynamic parameters used in the model can be easily accessed from thermodynamic databases via CALPHAD packages, such as Thermo-Calc[46] and Pandat [47]. The model predictions were validated by experimental data. In addition, the model was also extended to ternary system. For eutectic systems, the extended solid solubility was also calculated using the T_0 line and compared with the predictions of the developed model. The result of this work can help explain the appearance of non-equilibrium phases as well as the phenomena related to the extended solubility in rapid solidification processes. In addition, it can be easily adopted to design novel alloys for rapid solidification processes such as fusion-based metal AM.

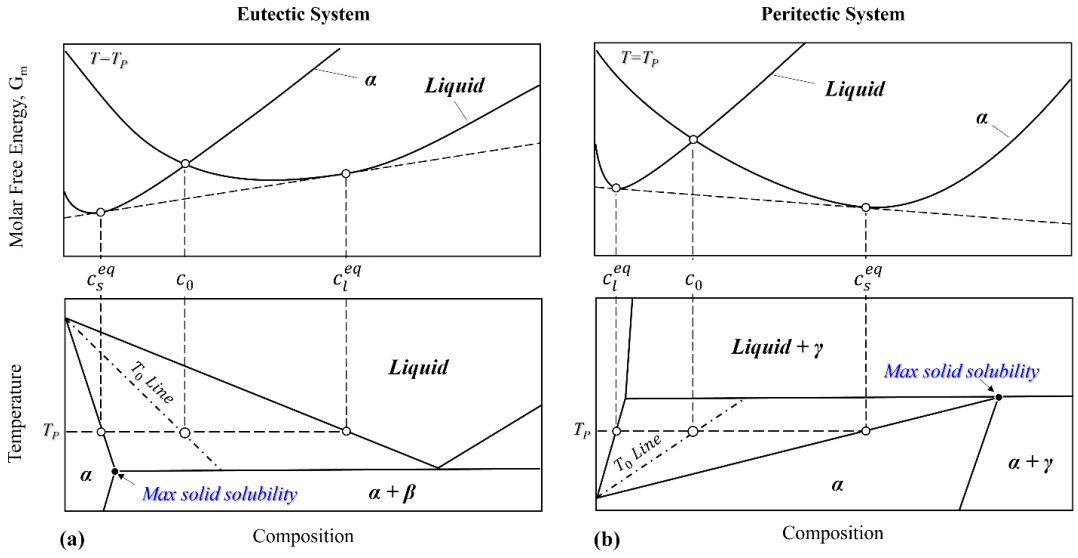

Figure 1. Schematic phase diagrams and corresponding molar free energies of solid solution α phase and liquid phase at $T = T_P$ for eutectic (a) and peritectic system (b). c_s^{eq} and c_l^{eq} are equilibrium solid composition and liquid composition at $T = T_P$, respectively.

2. MODEL

Since our new model is developed based on Shao and Tsakiropoulos's model [45], let us review their work first. Based on the time-dependent nucleation theory (TDNT), Shao and Tsakiropoulos derived the incubation time τ as follows (Eq. 14 in the original paper [45]).

$$\tau = \frac{7.2Rf(\theta)}{1-\cos\theta} \cdot \frac{a^4}{x_{\mathrm{L,eff}}\, d_a^2} \cdot \frac{T_r}{D\Delta S_m\, \Delta T_r^2} \tag{1}$$

where R is the gas constant, $f(\theta) = \frac{1}{4}(2 - 3\cos\theta + \cos^2\theta)$, θ is the contact angle for heterogeneous nucleation, $T_r = T/T_M$, T is the temperature, T_M is the melting temperature of the solid phase, $\Delta T_r = 1 - T_r$, ΔS_m is the molar entropy of fusion, a is the atomic jump distance, d_a is the average atomic diameter of the solid phase, and $x_{\mathrm{L,eff}}$ is the effective alloy concentration[45]. For a binary A-B system, $x_{\mathrm{L,eff}}$ is taken as $x_{\mathrm{L,A}}/x_{\mathrm{S,A}}$ when the composition of the nucleus is rich in A, where $x_{\mathrm{L,A}}$ and $x_{\mathrm{S,A}}$ stand for molar fraction of A in liquid and solid phase respectively. The average atomic diameter d_a can be calculated from molar weight w_m and density ρ of the solid phase via

$$d_a = \left(\frac{w_m}{\rho N_0}\right)^{1/3} \tag{2}$$

where $N_0$is the Avogadro's number. To calculate the diffusivity D, Shao and Tsakiropoulos [45] applied the Stokes-Einstein relationship[48],

$$\frac{\eta D}{T} = \frac{k}{6d_{a,L}} \tag{3}$$

where η is the viscosity of the melt and $d_{a,L}$ is the average distance between the liquid atoms and can be taken the same as d_a approximately. The above is the original model developed by Shao and Tsakiropoulos in 1994. The model has remained the same since. The viscosity η and diffusivity *D* are kinetic parameters that are not easily accessible. (Although the CALPHAD mobility databases of the major alloy systems are available, they are much less popular than thermodynamic databases and costly.) In the following, we derive our new model that is not dependent on any kinetic parameters.

As η is a function of temperature T only, Eq. (3) gives $Dd_a = kT/6\eta$, which can be regarded the same for all the nucleating phases. Thus, Eq. (1) can be simplified as

$$\tau = c \cdot \frac{1}{x_{\mathrm{L,eff}}\, d_a} \cdot \frac{T_r}{\Delta S_m\, \Delta T_r^2} \tag{4}$$

where $c = \frac{43.2 f(\theta) a^4 \eta}{(1-\cos\theta) N_0 T}$ is the same constant for all the phases.

At the critical temperature T (or the critical undercooling ΔT) when two competing nucleating phases have the same incubation time, we have $\tau_1 = \tau_2$, i.e.

$$\frac{1}{x_{\mathrm{L},1}\, d_{a1}} \cdot \frac{T_{r1}}{\Delta S_{m1}\, \Delta T_{r1}^2} = \frac{1}{x_{\mathrm{L},2}\, d_{a2}} \cdot \frac{T_{r2}}{\Delta S_{m2}\, \Delta T_{r2}^2} \tag{5}$$

where subscripts 1 and 2 stand for the matrix phase and the first solidifying intermetallic phase, respectively, $x_{\mathrm{L},1}$ and $x_{\mathrm{L},2}$ are the effective alloying concentration for each phase. The constant $\boldsymbol{c}$ containing viscosity η is now cancelled out. Hence, the model only has the thermodynamic parameters for both competing phases. The thermodynamic parameters, such as T_{M1}, T_{M2}, ΔS_{m1}, and ΔS_{m2}, can be assessed from CALPHAD databases. As the density of the solid phase is generally available[49], the average atomic diameter d_a is also accessible using Eq. (2). Thus, by *solving Eq. (5), the critical*

composition (x_A, or solubility limit for the case of a eutectic system) is calculated as a function of temperature T. In other words, for any given temperature T, there is a composition x_A when the two competing phases have the same incubation time τ. So, this composition x_A is the solubility for this temperature T. Then, the undercooling ΔT is calculated as the difference between the equilibrium liquidus of the alloys system of composition x_A,T_l, and T, *i.e.*, $\Delta T = T_l - T$. Since each x_A corresponds to one ΔT, a diagram of solubility vs. undercooling (or a phase diagram of undercooling and composition) can be established. This model is derived based on Shao and Tsakiropoulos's TDNT model [45], but it does not contain any ambiguous kinetic parameters anymore, which makes the model more feasible and reliable for explaining phase selection in AM and other rapid solidification processes**.** In APPENDIX, we use Al-Cr as an example to show how to use this model to calculate the solubility as a function of undercooling step by step.

3. RESULTS AND DISCUSSION

In this study, we chose Al alloys to test the model considering the availability of experimental data and the importance of extended solubility for strengthening Al alloys. The thermodynamic data obtained from the CALPHAD Al databases, including the entropy of fusion and transition temperature of competing phase, are shown in Table 1. It should be noted that the values of entropy of fusion ΔS_m assessed from commercial CALPHAD packages are different from Shao and Tsakiropoulos's original work [45]. As the CALPHAD method becomes much more developed over the last a few decades, the

thermodynamic data we used here should be more reliable. In the following we apply the developed model to calculate the phase selection and extended solid solubility for binary eutectic systems (Section 3.1), binary peritectic systems (Section 3.2), and a ternary system (Section 3.3).

Table 1. Typical values of thermodynamics property of α-Al and Intermetallic phases from Thermo-Calc (TCAL7), Pandat (PanAl), and Al-Ta database[50].

Phase	**Entropy of fusion, ΔS_m (Jmol^{-1}K^{-1})**	**Melting Temperature, T_M (K)**	**Density, ρ (g/cm^3)**
α-Al	11.47	933.47	2.70
$Al_{45}Cr_7$	18.13	1203.56	3.22
Al_6Mn	15.62	1111.95	3.32
$Al_{12}Mn$	15.62	992.44	3.02
Al_3Zr ($D0_{23}$)	15.52	1892.32	4.17
Al_3Ti($D0_{22}$)	13.74	1669.07	3.36
Al_3Sc($D0_{22}$)	15.57	1477.81	3.03
$Al_{13}Fe_4$	17.16	1427.85	3.84
Al_3Ta	17.90	1814.51	6.85
$Al_9Fe_2Si_2$	15.59	1089.07	3.69

3.1. BINARY EUTECTIC SYSTEMS

The binary eutectic systems evaluated in this study include Al-Mn, Al-Sc, and Al-Fe. Using the thermodynamic properties of each alloy obtained from CALPHAD packages (Table 1), the dependence of the solubility of different alloying elements on undercooling was evaluated using the new model. As shown in Figure 2, depending on the undercooling and the alloy composition, the solid solution α phase is stable on the upper left of the diagram with higher undercooling and lower alloy composition. In contrast, the intermetallic phase is stable with higher composition and lower undercooling. The phase boundary between α and the intermetallic phase defines the maximum solubility of the alloying element in the solid solution for a given undercooling. It can be seen from the diagrams that the critical undercooling required to suppress the nucleation of the primary intermetallic phase increases with the alloying composition. To achieve higher solid solubility, larger undercooling is required. In the modeling process, several intermetallic phases may be stable and need to be evaluated individually to determine the most stable intermetallic phase. For instance, in Al-Mn systems, Al_6Mn, $Al_{12}Mn$, and other Al-Mn compounds may solidify directly from the liquid. We evaluated the most stable two, Al_6Mn and $Al_{12}Mn$, and plotted them in Figure 2(a). As the Al_6Mn phase boundary lies higher than the $Al_{12}Mn$ phase boundary, Al_6Mn requires more undercooling to suppress from formation the liquid than $Al_{12}Mn$ for any given composition. Therefore, Al_6Mn is the stable intermetallic phase for the binary Al-Mn system. The model predictions of the Al-Mn system were compared with experimental data [51], which indicates good agreement. The kinks on the calculated phase boundaries correspond to the equilibrium eutectic composition. The Al-Sc binary

system, as another eutectic example, was explored. The calculated solid solubility versus undercooling is shown in Figure 2(b).

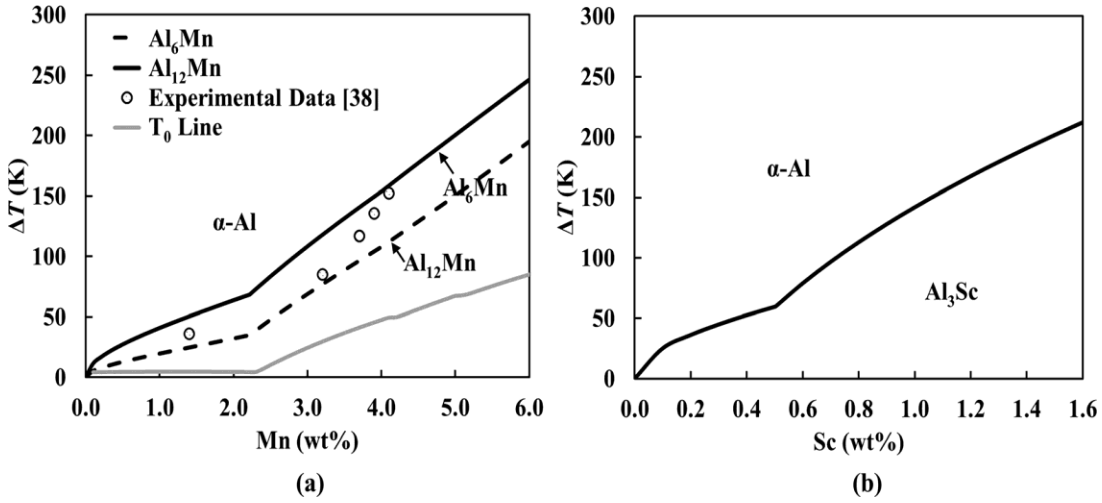

Figure 2. (a) Critical undercooling of the competing phase in Al-Mn binary system, (b) Critical undercooling of the competing phase in Al-Sc binary system.

The maximum solid solubility for a given undercooling in the Al-Mn alloy system was also calculated using the T_0 line method. As shown in Figure 2(a), the solubility calculated using this method shows a similar trend of the solubility dependence on undercooling. However, the predicted solubility is much higher than our model predictions as well as the experimental measurements. This is due to the T_0 line approach being a thermodynamic model in nature, which fails to consider the kinetic nucleation process. Therefore, it defines the theoretical maximum solid solubility that may be impossible to achieve.

3.2. BINARY PERITECTIC SYSTEMS

The peritectic forming elements such as Cr and Zr are important dispersoid formers to control the grain structures of Al alloys. However, their solubilities are exceptionally low, which significantly limits the operation window in casting and the following heat treatment. The formation of large primary intermetallic phases such as $Al_{45}Cr_7$ and Al_3Zr in casting is extremely deleterious to mechanical properties such as elongation and fracture toughness. Therefore, increasing the solid solubility of those peritectic forming elements is of great importance to the development of Al alloys.

The binary peritectic systems modeled in this study include Al-Cr, Al-Ti, Al-Zr, and Al-Ta. The diagrams of undercooling against the mass concentration of alloying elements Cr and Zr are shown in Figure 3(a) and (b), respectively. Similar to eutectic systems, the extended solid solubility in peritectic systems is found to increase monotonically with undercooling. In the Al-Cr system, it is found that $Al_{45}Cr_7$ is the stable intermetallic phase, which is consistent with Shao and Tsakiropoulos's work ($Al_{13}Cr_2$) [45]. As shown in Figure 3(a and b), the model predictions agree well with experimental data by Ichikawa et al [51]. It should be emphasized that the parameters used in this work were taken from CALPHAD packages (Table 1), and lattice parameters from the literature. None of the parameters are from fitting. Therefore, such good agreements indicate that the developed new model grasps the essence of phase selection and is reliable in the predictions of extended solid solubilities under large undercoolings.

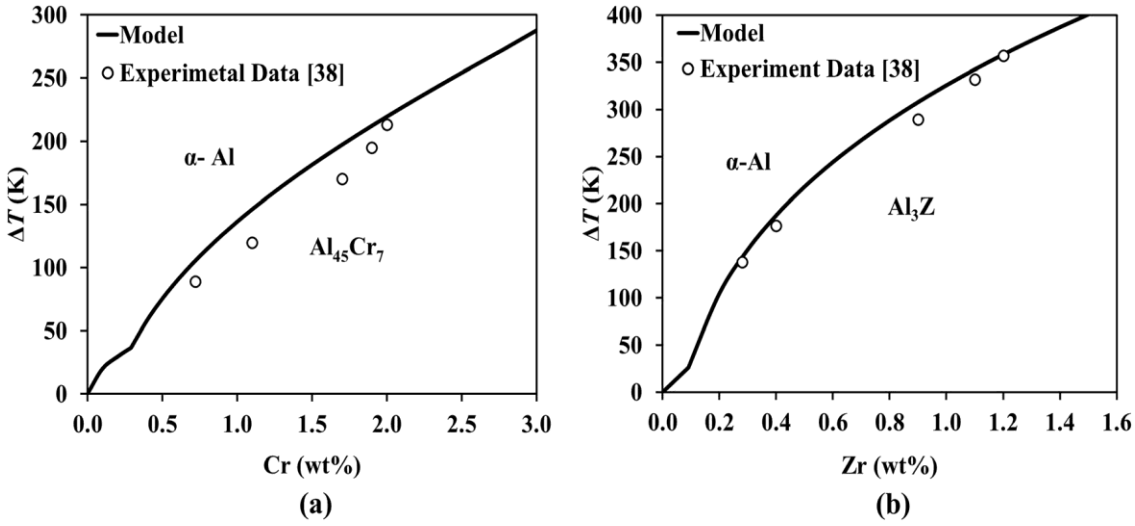

Figure 3. (a) Critical undercooling of the competing phase in Al-Cr binary system, (b) Critical undercooling of the competing phase in Al-Zr binary system.

To further understand the dependence of the solid solubility on undercooling, the relationship between the degree of supersaturation(c/c_e) and undercooling of various alloying elements in Al is shown in Figure 4. Supersaturation of the alloying element in the solid solution can be evaluated by comparing each supersaturated solubility c with the maximum solubility of the alloy at equilibrium (c_e) [51]. The degree of supersaturation determines the potential of solute species in the matrix phase (α-Al solid solution) to form intermetallic phases. Therefore, it is closely related to the potential of precipitation strengthening. It is also related to the impurity tolerance for elements like Fe and Mn.

The plot shows that the supersaturation degree of eutectic forming elements (Fe, Sc, and Mn) tend to increase faster with undercooling than the peritectic forming elements (Ti, Zr, and Cr). At undercooling temperature of 100K, almost all the eutectic alloys have doubled

their supersaturation, while the peritectic alloys still need to be saturated in the solid solution phase.

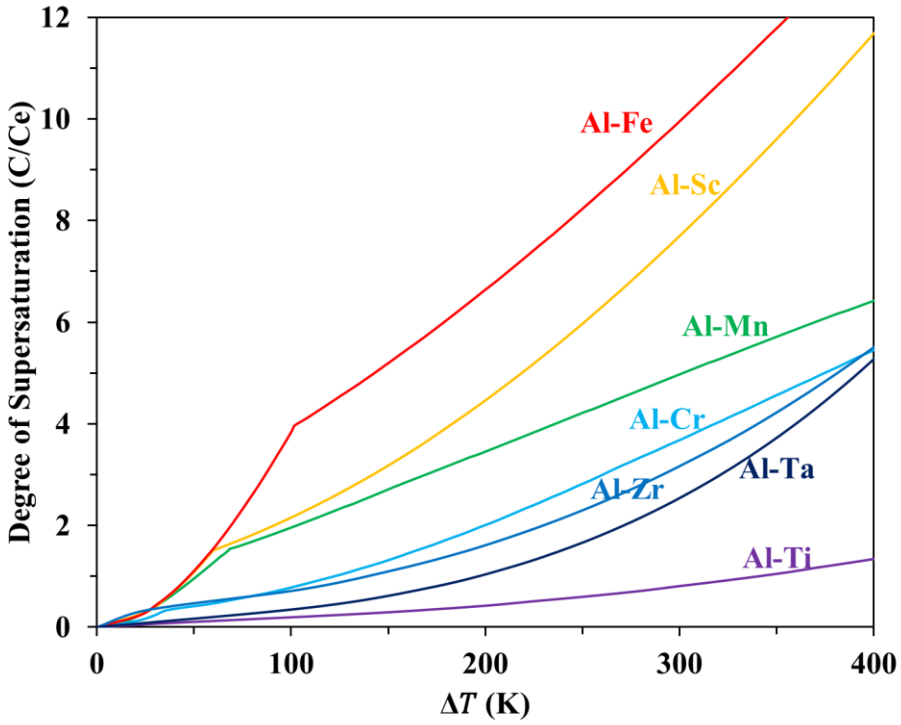

Figure 4. Degree of supersaturation (c/c_e) as a function of undercooling (ΔT) for Fe, Sc, Mn, Cr, Zr, Ta, and Ti.

3.3. TERNARY SYSTEMS

The developed model can also be applied to predict the phase selection of ternary compounds (or compounds containing even more elements) in the undercooled melt assuming the nucleation process is limited by only one element for a given composition. In this subsection, we use the β-AlFeSi intermetallic phase ($Al_9Fe_2Si_2$) as an example to demonstrate the applicability of the developed model.

Al-Si alloys are among the most widely used aluminum alloys, especially in the automobile industry, due to their excellent castability and mechanical properties[52], [53]. Al-Si-based alloys such as AlSi10Mg have also been adopted in the AM thanks to their outstanding resistance to cracking. Due to the presence of impurity iron, which is a result of the Bayer refining process [54], Al-Si alloys tend to form Al-Fe-Si ternary compounds. Among those complex compounds, the β-AlFeSi intermetallic phase is reported as one of the most deleterious phases in Al-Si alloys [55]. For instance, the formation of brittle β-AlFeSi due to high Fe contents in recycled alloys limits the use of secondary aluminum for structural components in the automotive industry. It was found that rates β-AlFeSi can be suppressed in casting by adding Mn and changing cooling [56], [57]. However, the mechanism is still not well understood. In addition, the increased tolerance of impurity Fe in rapid solidification can significantly reduce the raw material cost for AM processes and improve the reusability of AM powders. Therefore, it is crucial to understand the phase stability for different undercoolings and extended solubility of Fe in Al-Si-Fe alloys for both recycling aluminum alloys and AM. Although several researchers have worked on the Al-Fe-Si ternary system[58], [59], none of them have explored the dependence of phase selection on undercooling.

To simulate the competing nucleation of the ternary β-AlFeSi phase and the matrix α-Al phase, we assume the slower diffuser (Fe in this system) is the limiting element. Therefore, although the model is developed for binary, it can be extended to ternary and multi-component phases. By applying Eq. (5), we calculated the phase selection diagram of β-AlFeSi and α-Al phase as a function of undercooling. It can be seen from the contour plot (Figure 5a) that the undercooling required to suppress the

nucleation of β-AlFeSi shows different dependence on Fe and Si—the required undercooling increases dramatically with Fe. At the same time, it slowly decreases with the increasing Si concentration. Hence, for a given undercooling, increasing the Si content can increase the impurity tolerance of Fe. Our calculation also indicates that even a small undercooling can effectively suppress the formation of β-AlFeSi. For instance, for an undercooling of 100K, the Fe concentration can reach as high as 5wt%.

Additionally, the nucleation may also be limited by the scarcest species (Fe or Si depending on the given composition). As shown in the calculated diagram in Figure 5b, in the region above the dashed line, the nucleation is limited by Si concentration as it is less than Fe. Under the dashed line, the nucleation is limited by Fe concentration, which is the same as Figure 5a. However, experiments are needed to validate the models for ternary systems. The applicability of the model to quaternary and multicomponent alloy system needs further investigation.

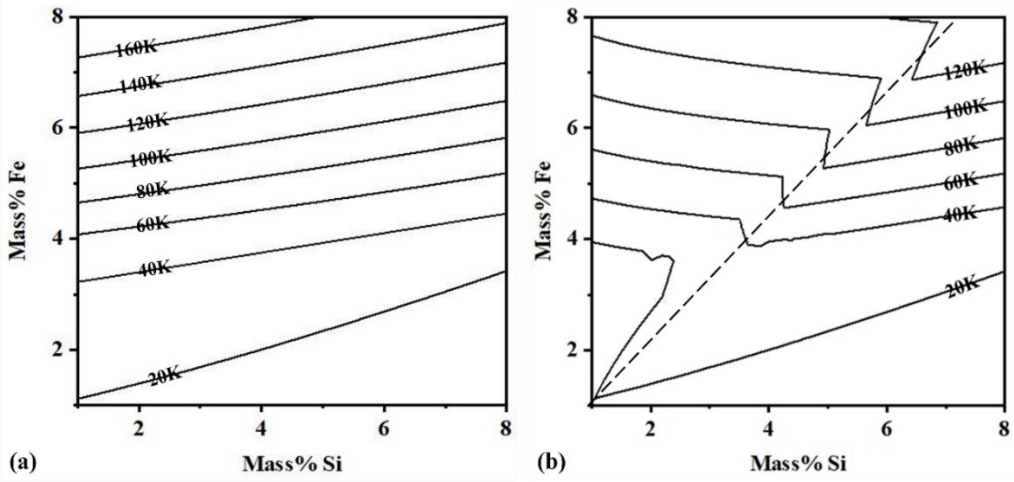

Figure 5. Calculated critical undercooling as a function of Fe and Si concentration (wt%) by assuming the nucleation is limited by (a) slower diffuser (Fe) or limited by (b) scarcest species. The dashed line indicates the change of limiting elements.

3.4. PRECIPITATION STRENGTHENING

One of the current directions of Al alloy development is the creep-resistant Al alloys for elevated temperature applications. Developing Al alloys to replace Ti alloys or superalloys for applications of around 300 °C may dramatically reduce the material and related processing costs. To achieve creep resistance at elevated temperatures, a large volume fraction of coherent precipitate phases is required. For instance, nickel-based superalloys that can withstand temperatures exceeding 75% of their melting point contain a high-volume fraction ($f \geq 0.5$) of precipitation phase γ', which is coherent with the matrix phase γ. According to the investigations by Knipling et al [60], Al_3M phase ($L1_2$-structure) formers, such as Ti, Hf, Zr, and Sc, are found to be the best candidates for developing creep-resistant Al alloys. However, the biggest hurdle for developing such types of Al alloys is their limited solubilities. For example, Ti, Zr, and Hf have liquid solubility less than 0.01at%, which significantly restricts the volume fraction of strengthening Al_3M phase one can achieve by casting.

Since rapid solidifications can significantly extend the solubility, we apply 200K undercooling to see how strong the Al alloys may become using those Al_3M phase formers. By applying the model, we found the volume fraction of Al_3M phases that may form under 200K undercooling is 0.04, 0.007, and 0.005 for Sc, Ti, and Zr, respectively. To evaluate the creep resistance, we calculate the Orowan stress [61] as a function of the size of the precipitate phase. The formula for calculating Orowan stress and the parameters can be found in the literature [60]. As shown in Figure 6, for the precipitates of 10 nm in radius, the Orowan stress for Al_3Sc ($f = 0.04$) is about 250 MPa, comparable to the yield strength of AA6061. Even for Al_3Ti ($f = 0.007$) and Al_3Zr ($f =$

0.005) the calculated Orowan stresses are nearly 100 MPa if the precipitate can be controlled to be around 10 nm in radius. Hence, in rapid solidification processes such as AM, the creep resistance can be dramatically improved by incorporating those elements. It should be noted that the resistance to coarsening is also critical for elevated temperature applications. It was found that the diffusivity of Ti and Zr at 400 °C are on the magnitude of 10^{-21} and 10^{-20} m^2 s^{-1} [60], indicating strong resistance to coarsening. Even for Sc, which has a diffusivity on the magnitude of 10^{-17} m^2 s^{-1} at 400 °C, recent studies have shown remarkably high coarsening and creep resistance at 300°C[62][63][64]. Therefore, rapid solidification promises a new route for developing novel creep-resistant Al alloys by extending the solubility of Al_3M forming elements to achieve a high-volume fraction of strengthening precipitate phases.

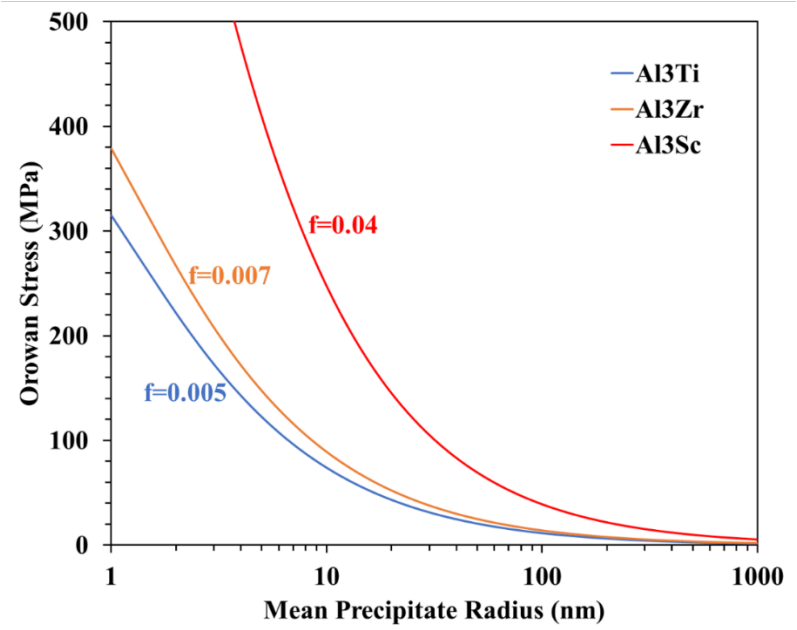

Figure 6. The Orowan stress as a function of the mean precipitate radius for various volume fraction for dispersed phases.

4. CONCLUSIONS

In this work, the phase selection model based on the time-dependent nucleation theory was modified to eliminate the dependence on diffusivity. The parameters needed by the new model can be easily accessed from CALPHAD packages and the physical property (density) database, which significantly improved the applicability and reliability of the model. The new model was applied to predict the extended solubility as a function of undercooling for various binary Al alloys. The predictions show good agreement with experiments. The T_0 line method, which is purely based on thermodynamics, neglected the kinetics of nucleation and hence overpredicts the solubilities. We demonstrated that the new model is also applicable to ternary and multicomponent phases, the solubility of which has never been theoretically studied before. This is very important since real alloys typically contain more than three elements. Lastly, the model was used to explore the possibility of developing creep-resistant Al alloys. It was found that 200 °C undercooling is sufficient to achieve decent high temperature strength by extending the solubility of Al_3M phase formers such as Ti, Zr, and Sc. This simple analytical model can be quickly adopted for analyzing the phase selection in rapid solidification experiments. It will also shed light on new alloy designs for rapid solidification processes like AM.

APPENDIX

In the following, we use Al-Cr binary system as an example to illustrate how to obtain the relationship between extended solid solubility and undercooling.

Identifying the first intermetallic phase ($Al_{45}Cr_7$) appearing in the Al-rich side of the equilibrium Al-Cr binary phase diagram.

Calculating d_a of both $Al_{45}Cr_7$ and α-Al from the density data[49] using Eq. (2).

Evaluating the melting temperature T_M and molar entropy of fusion ΔS_m for both $Al_{45}Cr_7$ and α-Al using Thermo-Calc. To simplify, we assume Al-x wt%Cr has the same melting temperature and entropy as pure Al. For low solute concentration, it is an acceptable assumption.

For each solubility value x, evaluating $x_{\mathrm{L,eff}}$, i.e., $x_{\mathrm{L},1} \approx 1.0$ (for small x), and

$$x_{\mathrm{L},2} = \frac{7x}{52}.$$

Substituting all the parameters in and solving Eq. (5) to obtain the critical temperature T.

Calculating undercooling corresponding ΔT for each solubility value x, using the liquidus temperature of Al-$x$wt%Cr obtained from Thermo-Calc (with database TCAL7).

ACKNOWLEDGEMENTS

The authors would like to thank the Senior Design team, K. Duncan, J. B. Fletcher, C. Simcoe, E. Klafehn, and H. Long, for practicing the model, experimental trials, and helpful discussions.

CONFLICT OF INTEREST

On behalf of all authors, the corresponding author states that there is no conflict of interest.

REFERENCES

[1] W. E. Frazier, "Metal additive manufacturing: A review," *J Mater Eng Perform*, vol. 23, no. 6, pp. 1917–1928, 2014, doi: 10.1007/s11665-014-0958-z.

[2] G. Shao and P. Tsakiropoulos, "Prediction of phase selection in rapid solidification using time dependent nucleation theory," *Acta Metallurgica Et Materialia*, vol. 42, no. 9, pp. 2937–2942, 1994, doi: 10.1016/0956-7151(94)90391-3.

[3] K. E. Knipling, D. C. Dunand, and D. N. Seidman, "Criteria for developing castable, creep-resistant aluminum-based alloys - A review," *International Journal of Materials Research*, vol. 97, no. 3, pp. 246–265, 2006.

[4] "Murray1982_Articles abt alimnum alloys.pdf."

[5] M. Asta, V. Ozolins, and C. Woodward, "A first-principles approach to modeling alloy phase equilibria," *Jom*, vol. 53, no. 9, pp. 16–19, 2001, doi: 10.1007/s11837-001-0062-3.

[6] T. W. Clyne, "Numerical treatment of rapid solidification," *Metallurgical Transactions B*, vol. 15, no. 2, pp. 369–381, 1984, doi: 10.1007/BF02667341.

[7] D. M. Herlach, "Reports: A Review Journal Non-equilibrium solidification of undercooled metallic melts," *Materials Science and Engineering*, vol. 12, pp. 177–272, 1994.

[8] E. Clouet, "Modeling of Nucleation Processes Thermodynamic Approach Conditions for Nucleation," vol. 22, no. Eq 2, pp. 203–219, 2009, [Online]. Available: www.asminternational.org

[9] W. J. Boettinger, S. R. Coriell, and R. F. Sekerka, "Mechanisms of micro segregation-free solidification," *Materials Science and Engineering*, vol. 65, no. 1, pp. 27–36, 1984, doi: 10.1016/0025-5416(84)90196-4.

[10] T. Ichikawa, Riei Ohashi, Teruo Ikeda, “Effects of Cooling Rate and Supercooling Degree on Solidified Structure of Al-Mn , Al-Cr and Al-Zr in Rapid Solidification,” *Transaction of the Japan Institute of Metals*, vol. 12, no. 5, pp. 280–284, 1971.

[11] I. Riei and O. Teruo, “Effects of the third additional elements on rapid cooled cast structures of Al-3∼5% Mn alloys,” *Journal of Japan Institute of Light Metals*, vol. 16, no. 6, pp. 304–311, 1966, doi: 10.2464/jilm.16.304.

[12] I. Riei and O. Teruo, “Effects of the third additional elements on rapid cooled cast structures of Al-3∼5% Mn alloys,” *Journal of Japan Institute of Light Metals*, vol. 16, no. 6, pp. 304–311, 1966, doi: 10.2464/jilm.16.304.

[13] M. R. Abul, R. F. Cochrane, and A. M. Mullis, “Microstructural development and mechanical properties of drop tube atomized Al-2.85 wt% Fe,” *J Mater Sci Technol*, vol. 104, pp. 41–51, 2022, doi: 10.1016/j.jmst.2021.05.085.

[14] W. E. Frazier, “Metal Additive Manufacturing: A Review,” *J Mater Eng Perform*, vol. 23, no. 6, pp. 1917–1928, Jun. 2014, doi: 10.1007/s11665-014-0958-z.

[15] D. Herlach, “Non-equilibrium solidification of undercooled metallic metals,” *Materials Science and Engineering: R: Reports*, vol. 12, no. 4–5, pp. 177–272, Aug. 1994, doi: 10.1016/0927-796X(94)90011-6.

[16] H. Jones, “The status of rapid solidification of alloys in research and application,” *J Mater Sci*, vol. 19, no. 4, pp. 1043–1076, 1984, doi: 10.1007/BF01120015.

[17] F. H. Froes, Y.-W. Kim, and S. Krishnamurthy, “Rapid solidification of lightweight metal alloys,” *Materials Science and Engineering: A*, vol. 117, no. C, pp. 19–32, Sep. 1989, doi: 10.1016/0921-5093(89)90082-8.

[18] D. Herlach, “Non-Equilibrium Solidification of Undercooled Metallic Melts,” *Metals (Basel)*, vol. 4, no. 2, pp. 196–234, Jun. 2014, doi: 10.3390/met4020196.

[19] K. Eckler, D. M. Herlach, R. G. Hamerton, and A. L. Greer, “Dendrite growth velocities in highly undercooled, dilute Ni-C melts,” *Materials Science and Engineering: A*, vol. 133, no. C, pp. 730–733, Mar. 1991, doi: 10.1016/0921-5093(91)90173-K.

[20] K. Eckler, R. F. Cochrane, D. M. Herlach, B. Feuerbacher, and M. Jurisch, “Evidence for a transition from diffusion-controlled to thermally controlled solidification in metallic alloys,” *Phys Rev B*, vol. 45, no. 9, pp. 5019–5022, Mar. 1992, doi: 10.1103/PhysRevB.45.5019.

[21] K. Eckler, A. F. Norman, F. Gärtner, A. L. Greer, and D. M. Herlach, "Microstructures of dilute Ni C alloys obtained from undercooled droplets," *J Cryst Growth*, vol. 173, no. 3–4, pp. 528–540, Apr. 1997, doi: 10.1016/S0022-0248(96)01066-4.

[22] K. Eckler and D. M. Herlach, "Measurements of dendrite growth velocities in undercooled pure Ni-melts—some new results," *Materials Science and Engineering: A*, vol. 178, no. 1–2, pp. 159–162, Apr. 1994, doi: 10.1016/0921-5093(94)90535-5.

[23] Y. Wu, T. J. Piccone, Y. Shiohara, and M. C. Flemings, "Dendritic growth of undercooled nickel-tin: Part I," *Metallurgical Transactions A*, vol. 18, no. 5, pp. 915–924, May 1987, doi: 10.1007/BF02646933.

[24] Y. Wu, T. J. Piccone, Y. Shiohara, and M. C. Flemings, "Dendritic growth of undercooled nickel-tin: Part II," *Metallurgical and Materials Transactions A*, vol. 18, no. 5, pp. 925–932, May 1987, doi: 10.1007/BF02646934.

[25] Y. Wu, T. J. Piccone, Y. Shiohara, and M. C. Flemings, "Dendritic Growth of Undercooled Nickel-Tin: Part III," *Metallurgical Transactions A*, vol. 19, no. 4, pp. 1109–1119, Apr. 1988, doi: 10.1007/BF02628395.

[26] A. Munitz, A. B. Gokhale, and R. Abbaschian, "Effect of supercooling on the microstructure of Al-Nb alloys," *J Mater Sci*, vol. 35, no. 9, pp. 2263–2271, 2000, doi: 10.1023/A:1004783011253.

[27] N. J. E. Adkins, N. Saunders, and P. Tsakiropoulos, "Rapid solidification of peritectic aluminum alloys," *Materials Science and Engineering*, vol. 98, no. C, pp. 217–219, Feb. 1988, doi: 10.1016/0025-5416(88)90158-9.

[28] M. G. Chu, A. Giron, and D. A. Granger, "Microstructure and heat flow in melt-spun aluminum alloys," in *Proc. ASM's Int. Conf. on Rapidly Solidified Materials*, Metals Park, OH, 1986, pp. 311–316.

[29] M. G. Chu and D. A. Granger, "Solidification and microstructure analysis of rapidly solidified melt-spun Al-Fe alloys," *Metallurgical Transactions A*, vol. 21, no. 1, pp. 205–212, Jan. 1990, doi: 10.1007/BF02656437.

[30] G. Waterloo and H. Jones, "Microstructure and thermal stability of melt-spun Al-Nd and Al-Ce alloy ribbons," *J Mater Sci*, vol. 31, no. 9, pp. 2301–2310, 1996, doi: 10.1007/BF01152938.

[31] J. Xu *et al.*, "Solidification behavior and microstructure of Ti-(37−52) at% Al alloys synthesized in situ via dual-wire electron beam freeform fabrication," *Additive Manufacturing*, vol. 46. 2021. doi: 10.1016/j.addma.2021.102113.

[32] Q. Tan *et al.*, “Demonstrating the roles of solute and nucleant in grain refinement of additively manufactured aluminum alloys,” *Additive Manufacturing*, vol. 49. 2022. doi: 10.1016/j.addma.2021.102516.

[33] M. Opprecht, J.-P. Garandet, G. Roux, and C. Flament, “An understanding of duplex microstructures encountered during high strength aluminum alloy laser beam melting processing,” *Acta Mater*, vol. 215, p. 117024, Aug. 2021, doi: 10.1016/j.actamat.2021.117024.

[34] F. Xiao *et al.*, “Niobium nanoparticle-enabled grain refinement of a crack-free high strength Al-Zn-Mg-Cu alloy manufactured by selective laser melting,” *J Alloys Compd*, vol. 900, p. 163427, Apr. 2022, doi: 10.1016/j.jallcom.2021.163427.

[35] Y. Wang *et al.*, “Laser powder bed fusion of Zr-modified Al–Cu–Mg alloy: Crack-inhibiting, grain refinement, and mechanical properties,” *Materials Science and Engineering: A*, vol. 838, p. 142618, Mar. 2022, doi: 10.1016/j.msea.2022.142618.

[36] Z. Wang *et al.*, “Laser-based directed energy deposition of novel Sc/Zr-modified Al-Mg alloys: columnar-to-equiaxed transition and aging hardening behavior,” *J Mater Sci Technol*, vol. 69, pp. 168–179, 2021, doi: 10.1016/j.jmst.2020.08.003.

[37] Q. Li *et al.*, “Development of a high strength Zr/Sc/Hf-modified Al-Mn-Mg alloy using Laser Powder Bed Fusion: Design of a heterogeneous microstructure incorporating synergistic multiple strengthening mechanisms,” *Addit Manuf*, vol. 57, p. 102967, Sep. 2022, doi: 10.1016/j.addma.2022.102967.

[38] Z. Wang *et al.*, “Laser powder bed fusion of high-strength Sc/Zr-modified Al–Mg alloy: phase selection, microstructural/mechanical heterogeneity, and tensile deformation behavior,” *J Mater Sci Technol*, vol. 95, pp. 40–56, Dec. 2021, doi: 10.1016/j.jmst.2021.03.069.

[39] Z. Wang, X. Lin, L. Wang, Y. Cao, Y. Zhou, and W. Huang, “Microstructure evolution and mechanical properties of the wire + arc additive manufacturing Al-Cu alloy,” *Addit Manuf*, vol. 47, p. 102298, Nov. 2021, doi: 10.1016/j.addma.2021.102298.

[40] M. Asta *et al.*, “Solidification microstructures and solid-state parallels: Recent developments, future directions,” *Acta Mater*, vol. 57, no. 4, pp. 941–971, Feb. 2009, doi: 10.1016/j.actamat.2008.10.020.

[41] W. Kurz, M. Rappaz, and R. Trivedi, “Progress in modelling solidification microstructures in metals and alloys. Part II: dendrites from 2001 to 2018,” *International Materials Reviews*, vol. 66, no. 1, pp. 30–76, 2021, doi: 10.1080/09506608.2020.1757894.

[42] P. K. Galenko and D. Jou, “Rapid solidification as non-ergodic phenomenon,” *Phys Rep*, vol. 818, pp. 1–70, Jul. 2019, doi: 10.1016/j.physrep.2019.06.002.

[43] J. C. Baker and J. W. Cahn, “Thermodynamics of Solidification,” in *The Selected Works of John W. Cahn*, Hoboken, NJ, USA: John Wiley & Sons, Inc., 2013, pp. 253–288. doi: 10.1002/9781118788295.ch26.

[44] J. L. Murray, “Thermodynamic Factors in the Extension of Solid Solubility in Al-Based Alloys,” *MRS Proceedings*, vol. 19, p. 249, Feb. 1982, doi: 10.1557/PROC-19-249.

[45] G. Shao and P. Tsakiropoulos, “Prediction of phase selection in rapid solidification using time dependent nucleation theory,” *Acta Metallurgical et Materialia*, vol. 42, no. 9, pp. 2937–2942, Sep. 1994, doi: 10.1016/0956-7151(94)90391-3.

[46] J.-O. O. Andersson, T. Helander, L. Höglund, P. Shi, and B. Sundman, “Thermo-Calc & DICTRA, computational tools for materials science,” *CALPHAD*, vol. 26, no. 2, pp. 273–312, Jun. 2002, doi: 10.1016/S0364-5916(02)00037-8.

[47] W. Cao *et al.*, “PANDAT software with Pan Engine, Pan Optimizer and Pan Precipitation for multi-component phase diagram calculation and materials property simulation,” *CALPHAD*, vol. 33, no. 2, pp. 328–342, Jun. 2009, doi: 10.1016/j.calphad.2008.08.004.

[48] J. A. Cahill and A. V. Grosse, “Viscosity and self-diffusion of liquid thallium from its melting point to about 1300°K,” *Journal of Physical Chemistry*, vol. 69, no. 2, pp. 518–521, 1965, doi: 10.1021/j100886a026.

[49] “https://materials.springer.com/.”

[50] V. T. Witusiewicz *et al.*, “Experimental study and thermodynamic re-assessment of the binary Al-Ta system,” *Intermetallic (Barking)*, vol. 18, no. 1, pp. 92–106, 2010, doi: 10.1016/j.intermet.2009.06.015.

[51] R. Ichikawa, T. Ohashi, and T. Ikeda, “Effects of Cooling Rate and Supercooling Degree on Solidified Structure of Al-Mn , Al-Cr and Al-Zr in Rapid Solidification,” *Transaction of the Japan Institute of Metals*, vol. 12, no. 5, pp. 280–284, 1971.

[52] L. Y. Zhang *et al.*, “Effect of cooling rate on solidified microstructure and mechanical properties of aluminium-A356 alloy,” *J Mater Process Technol*, vol. 207, no. 1–3, pp. 107–111, 2008, doi: 10.1016/j.jmatprotec.2007.12.059.

[53] J. A. Taylor, “Iron-Containing Intermetallic Phases in Al-Si Based Casting Alloys,” *Procedia Materials Science*, vol. 1, pp. 19–33, 2012, doi: 10.1016/j.mspro.2012.06.004.

[54] J. A. Taylor, “Iron-Containing Intermetallic Phases in Al-Si Based Casting Alloys,” *Procedia Materials Science*, vol. 1, pp. 19–33, 2012, doi: 10.1016/j.mspro.2012.06.004.

[55] W. S. Ebhota and T.-C. Jen, “Intermetallics Formation and Their Effect on Mechanical Properties of Al-Si-X Alloys,” *Intermetallic Compounds - Formation and Applications*, 2018, doi: 10.5772/intechopen.73188.

[56] E. Cinkilic, C. D. Ridgeway, X. Yan, and A. A. Luo, “A Formation Map of Iron-Containing Intermetallic Phases in Recycled Cast Aluminum Alloys,” *Metallurgical and Materials Transactions A*, vol. 50, no. 12, pp. 5945–5956, Dec. 2019, doi: 10.1007/s11661-019-05469-6.

[57] E. Cinkilic, M. Moodispaw, J. Zhang, J. Miao, and A. A. Luo, “A New Recycled Al–Si–Mg Alloy for Sustainable Structural Die Casting Applications,” *Metallurgical and Materials Transactions A*, vol. 53, no. 8, pp. 2861–2873, Aug. 2022, doi: 10.1007/s11661-022-06711-4.

[58] M. Yildirim and D. Özyürek, “The effects of Mg amount on the microstructure and mechanical properties of Al-Si-Mg alloys,” *Mater Des*, vol. 51, pp. 767–774, 2013, doi: 10.1016/j.matdes.2013.04.089.

[59] W. S. Ebhota and T.-C. Jen, “Intermetallics Formation and Their Effect on Mechanical Properties of Al-Si-X Alloys,” in *Intermetallic Compounds - Formation and Applications*, InTech, 2018. doi: 10.5772/intechopen.73188.

[60] K. E. Knipling, D. C. Dunand, and D. N. Seidman, “Criteria for developing castable, creep-resistant aluminum-based alloys – A review,” *Zeitschrift für Metallkunde*, vol. 97, no. 3, pp. 246–265, Mar. 2006, doi: 10.3139/146.101249.

[61] J. F. Nie and B. C. Muddle, “Microstructural design of high-strength aluminum alloys,” *Journal of Phase Equilibria*, vol. 19, no. 6, pp. 543–551, Dec. 1998, doi: 10.1361/105497198770341734.

[62] M. E. van Dalen, D. C. Dunand, and D. N. Seidman, “Effects of Ti additions on the nanostructure and creep properties of precipitation-strengthened Al–Sc alloys,” *Acta Mater*, vol. 53, no. 15, pp. 4225–4235, Sep. 2005, doi: 10.1016/j.actamat.2005.05.022.

[63] D. N. Seidman, E. A. Marquis, and D. C. Dunand, “Precipitation strengthening at ambient and elevated temperatures of heat-treatable Al(Sc) alloys,” *Acta Mater*, vol. 50, no. 16, pp. 4021–4035, Sep. 2002, doi: 10.1016/S1359-6454(02)00201-X.

[64] E. MARQUIS, D. SEIDMAN, M. ASTA, and C. WOODWARD, “Composition evolution of nanoscale AlSc precipitates in an Al-Mg–Sc alloy: Experiments and computations,” *Acta Mater*, vol. 54, no. 1, pp. 119–130, Jan. 2006, doi: 10.1016/j.actamat.2005.08.035.

SECTION

3. EXPERIMENT

This section explains the experiments using a wedge copper mold to obtain different cooling rates. However, capturing the temperatures during rapid cooling is challenging. Therefore, two different methods were employed: fiber grating sensors (FBGs) and a K-type thermocouple. However, both methods have their issues. Also, the microstructure of the thinner section was analyzed for the different phases and the secondary dendrite arm spacing of dendrites.

3.1. EXPERIMENTAL PROCEDURE

Copper mold was selected for the experiment due to its excellent thermal conductivity. The copper mold with dimensions 3” x 3” x 6” for the experiment was fabricated at the departmental machine shop laboratory. The wedge shape of the cast and the mold cavity are represented in Figure 3.1. The mold cavity was wedged to capture changes in temperature, cooling rate, and the microstructure at various positions in the mold. The bottom of the wedge has the thinnest section and extracts heat quickly due to the small surface area, and the thickness of the mold is highest at this point. A small passage of air is allowed to avoid shrinkage defects. The experimental procedure for casting the aluminum alloy ingots consists of a box furnace, a 25 mL alumina crucible, ~50 g of charge material, a graphite stir rod, a graphite skimming tool, the copper wedge mold, a bucket of water, a water pump and four rubber hoses. The pump was inserted into the

bucket of water, and the hoses were attached to the pump and water-cooling channels. When the 10 minutes of stirring was complete, the pump was turned on to circulate water around the copper mold. The aluminum alloy was depressed with the graphite stir rod to remove the oxides before being poured into the copper mold. The water-cooled system surrounding the mold consists of a small hand centrifugal pump, hose, and clips. The water-cooled system was installed appropriately to ensure no water leakage or moisture in contact with the liquid aluminum alloy, as it is volatile, and for fast heat removal during the pouring of molten aluminum alloys.

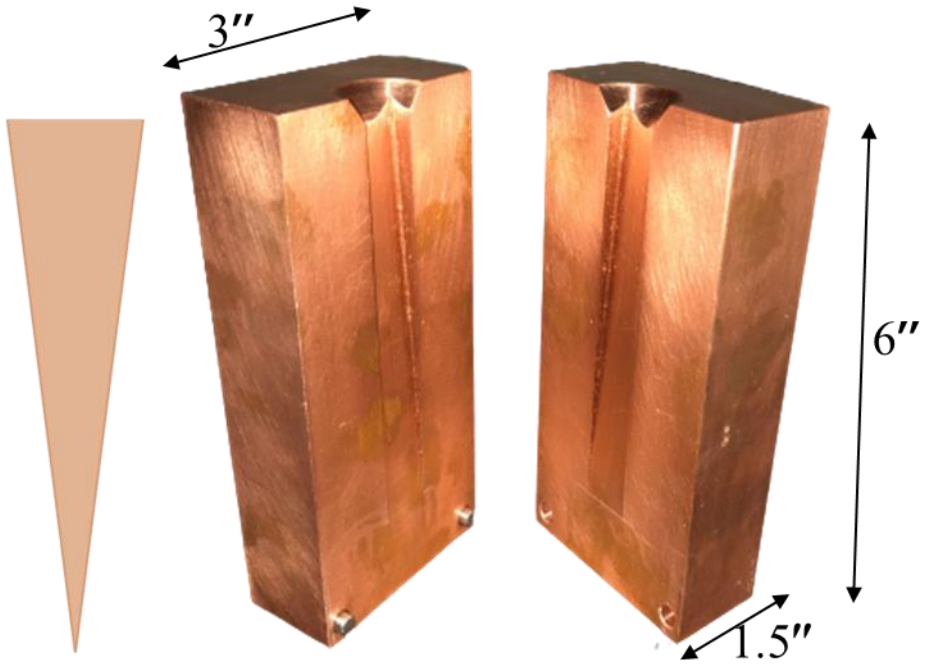

Figure 3.1: The copper wedge mold consists of two halves joined to make a block.

The furnace was first used for preheating the tongs, stir rod, and mold at 130 ℃ for 30 minutes to drive off water because molten aluminum alloy explodes in contact with moisture. It was then ramped up to the melting temperature set to 100℃ above the

liquidus temperature of the evaluated composition. The alumina crucible with the charge material was inserted into the melting furnace. A thermocouple was used to periodically check the melting temperature during the alloy's melting inside the crucible. Once the thermocouple reads the target temperature, the crucible was regularly stirred with the graphite stir rod for 10 minutes to homogenize the chemistry and ensure complete melting of the intermetallic phases.

The solidified poured samples were cut into sections using the slow band saw with an appropriate cutting disc. The solidified wedge alloy shown in Figure 3.1 was typically sectioned into slices, with each slice having a possibly different microstructure and grain size due to the thickness and position of the slice. The polishing and etching procedures were obtained from ASTM E407, which gives general polishing and etching procedures for several materials. A method for Al alloy was chosen, and this required very dilute HF (1mL HF / 200 mL water) swabbed with cotton wool along the surface for 15s but varies with regards to the alloys; for example, Al-4.5wt% Cu wedges may be etched for the 30s, whereas the Al-Cr samples were etched for about 1 minute (and they still appeared under-etched). These times were based on the appearance of the expected microstructure, i.e., if dendrites were visible in the Al-Cu samples, they were considered etched. Al-Cr was swabbed for over 1 minute until we achieved a clear visible dendrite and a better microstructure from the different pour of aluminum alloys.

Optical Microscopy was used to study the microstructure of the phases present in all the solidified aluminum alloys for every slice we sectioned. Image J software measured the dendritic structure's secondary dendrite arm spacing. The cooling rate of

different solidified alloy sections was estimated by subtracting measured temperatures for various positions.

3.1.1. Using Fiber Bragg Grating Sensors (Fbgs). Numerous approaches have been used to study the solidification characteristics of different alloys during mold casting. Thermal analysis techniques, X-ray Microtomography, and other techniques have been used in past studies to capture the solidification characteristics during casting. Cooling rates at various positions inside the mold during casting are known to be different; hence, the solidification characteristics at other positions are different during the casting process. This limits the process mentioned above as they focus on a one-point measurement rather than a multi-point one. Fiber Bragg Grating Sensors (FBGs) as an optic-fiber method have been widely used to study the strain behavior during casting. FBGs are an example of grating-based devices whose basic principle of operation is to monitor the change in wavelength of the returned Bragg signal with the changes in the strain or temperature measured. Several authors explained explicitly the experimental preparation of the FBGs, which consist of a supercontinuum laser source (SC-5, Wuhan Yangtze Soton Laser) with a wavelength range of 400-2200nm, a Bayspec multimode interrogator integrated with a laptop, and a 3 dB multimode coupler to acquire the reflection spectra of the FBG array. The schematic diagram of the multi-mode FBGs is shown in Figure 3.2a below. FBG 7 corresponds to the thinnest part of the solidified alloy, while FBG 1 represents the thickest section. Each sensor is placed 5mm apart to capture the temperature inside the copper mold at different positions. The fiber is placed in a stainless tube dipped into the mold cavity's center to capture the temperature changes during solidification. The solidified aluminum alloys with fiber embedded in a stainless

tube are shown in Figure 3.2b below, which gives an overview of the experimental setup using FBGs.

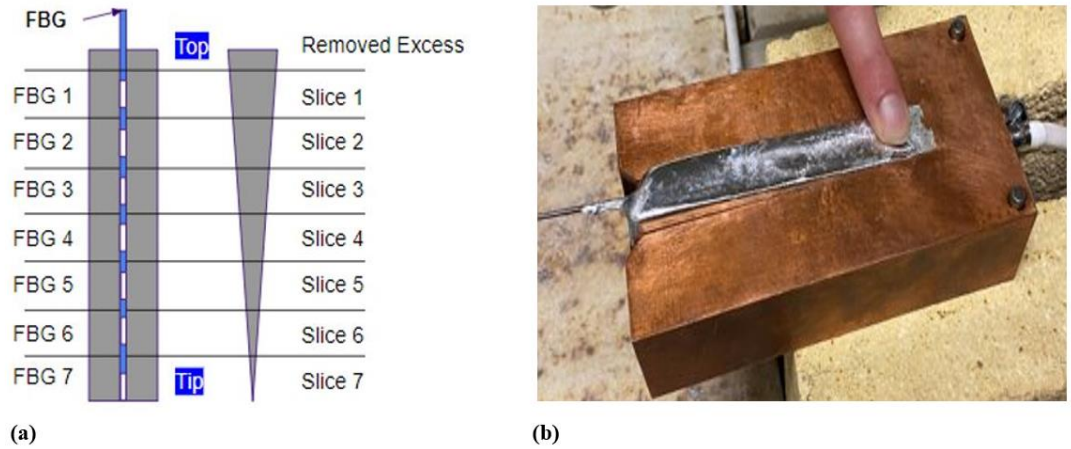

Figure 3.2: a) Front and side profiles of the wedge with indicated cut lines b) Half copper mold section with solidified alloy sample and FBG.

3.1.2. Using Data Acquisition and Oscilloscope. The data acquisition system consists of a transducer amplifier, thermocouple wire, male and female connectors, cold junction at 0ºC for reference temperature point, and oscilloscope. The schematic experimental setup is shown in Figure 3.3. The K-type thermocouple has an exposed tip to respond quickly to changes in temperature compared to the grounded type. The k-type thermocouple was connected through a k-type thermocouple wire to the cold junction containing ice water at 0ºC. The cold junction compensates for the missing thermoelectric voltage because the thermocouple end is not at 0ºC. The cold junction is connected to the amplifier transducer through a 7-way pin circular connector. The BNC-type connector was used to connect the oscilloscope with the amplifier transducer with predefined

configurations. The amplifier increases the amplitude of the signal captured by the thermocouple, producing a proportionally greater amplitude signal at its output. The oscilloscope acquires the amplified voltage and converts it to digital data and a waveform. The amplifier transducer is, in turn, connected to the oscilloscope, which captures the amplified voltage, converts it to digital data and a waveform through the trigger mode, and later saves it on a computer as a CSV file for conversion into temperature values using the standard temperature table and MATLAB software. Figure 3.4 depicts the redesigned copper mold with holes bored into it for four different K-type thermocouples to capture the solidification temperature of molten alloys. The K-type thermocouple is made to fit into the hole with the tip at the center of the mold cavity. Cooling rate and undercooling can be deduced from the data obtained from the experiment, which will be used to validate our model.

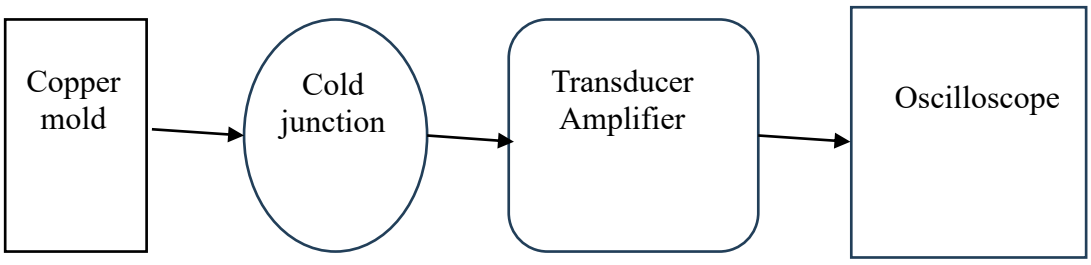

Figure 3.3: Schematic of my proposed experimental setup.

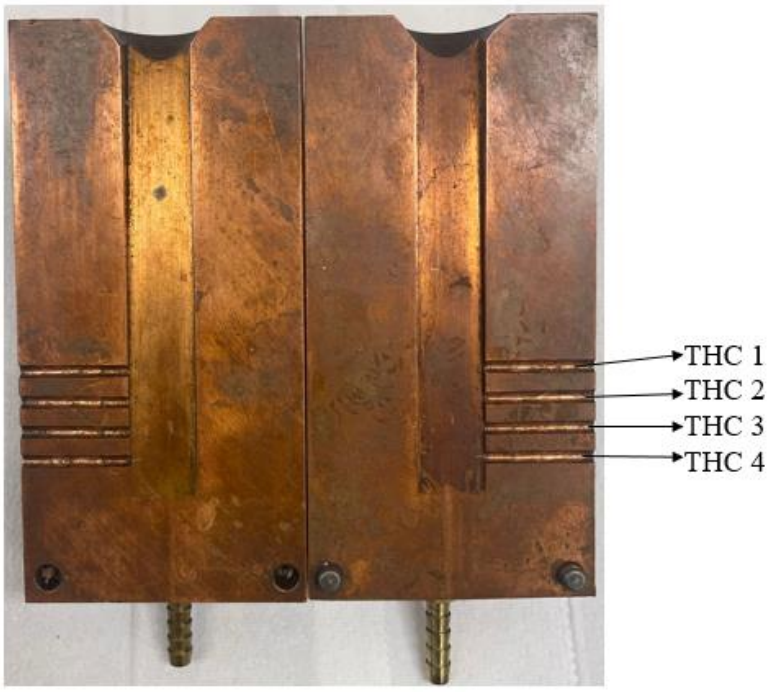

Figure 3.4: Copper mold with machined K-type thermocouple hollow.

3.2. RESULTS AND DISCUSSIONS

The temperature vs. time graph for the aluminum alloy Al-4.5wt%Cu used for the experiment is shown below in Figure 3.5a. FBG 1 to 7 shown in Figure 3.2a represent the FBGs on the fiber at different positions during the experiment, which capture the temperature changes during the rapid solidification process. The FBGs captured the freezing range from 654ºC to 552ºC as indicated by the FBG 2 and FBG 7, respectively, of the alloy, which is approximately the liquids (649ºC) and solidus (564ºC) temperature, respectively, as seen in Figure 3.5a. The pouring temperature was around 850ºC before pouring into the rapidly cooled copper mold. However, the curve is inconsistent with the position of the sensors on the fiber with temperature values. The starting temperature of each FBG is inconsistent. Also, the fiber sensors should be sequential from FBG 1 to

FBG 7, as positioned in Figure 3.2a. This suggests that the experimental setup has some challenges, such as the stainless tube, which houses the fiber sensor, and the sensor's indirect contact with the copper mold. This can also result from the sensitivity or calibration of the fiber sensor, the small mold cavity, or the alloy being poured. Also, the inhomogeneity of the alloy with the presence of intermetallic may be a problem during the pouring. The cooling rate vs. time graph is also depicted in Figure 3.5b, which is an equivalent of the temperature vs. time graph and does not give the copper mold's consequential cooling rate. The thinnest section (FBG 7) is expected to have the fastest cooling rate. The slowest cooling rate should correspond to FBG 1. However, the highest cooling rate is 238K/sec and was given by FBG 1. This is evident from the previous plot, as the cooling rate is calculated by subtracting the temperature difference of each fiber sensor per second. An optical micrograph of the alloy cast using optical microscopy is shown below in Figure 3.6, which was obtained after careful metallographic preparation and using HF etchant. Figure 3.6a, which corresponds to the tip of the Al-Cu alloy, shows a columnar dendritic microstructure with average secondary dendrite arm spacing (SDAS) of around 9µm to 23µm, respectively. A fine microstructure is expected at the mold wall or boundary, and a smaller columnar dendritic or equiaxed microstructure further away and to the center of the mold. The dark color at the grain boundaries suggests either a primary intermetallic compound or an undissolved compound. However, due to the high solubility of Cu in Al, it's unclear if it's an undissolved intermetallic compound. Figure 3.6b shows the Al-Cr microstructure, like the previous one. As suggested in both images, there are no dramatic changes in the microstructure. It seems the molten alloy has solidified before getting to the bottom of the mold. The

microstructure indicates that the molten was not in contact with the mold. Undissolved primary intermetallic compounds in Al-Cr may cause the dark area due to the low solubility of Cr in Al. It can also be a result of undissolved compounds in the alloy.

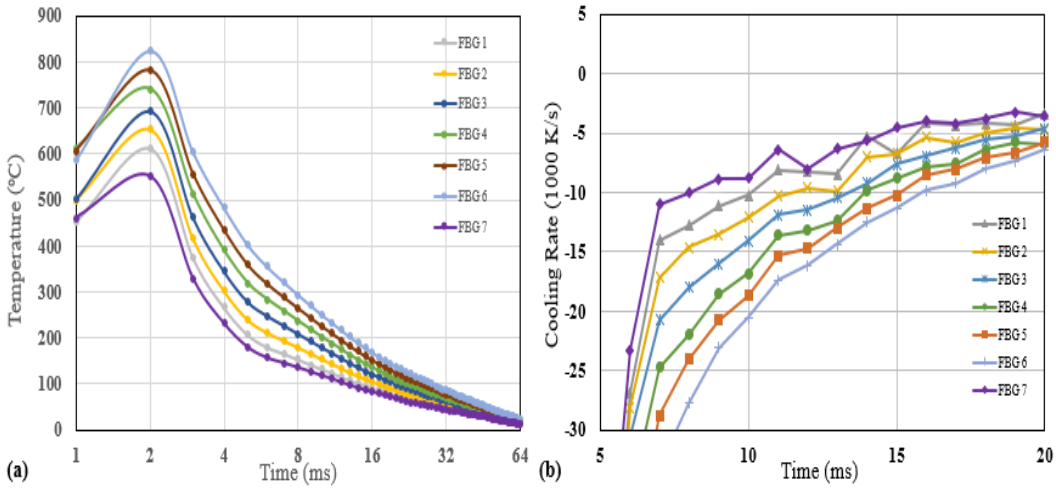

Figure 3.5: a) Temperature vs. time graph for Al-4.5wt%Cu with non-uniform data b) Cooling rate vs. time graph for Al-4.5wt%Cu.

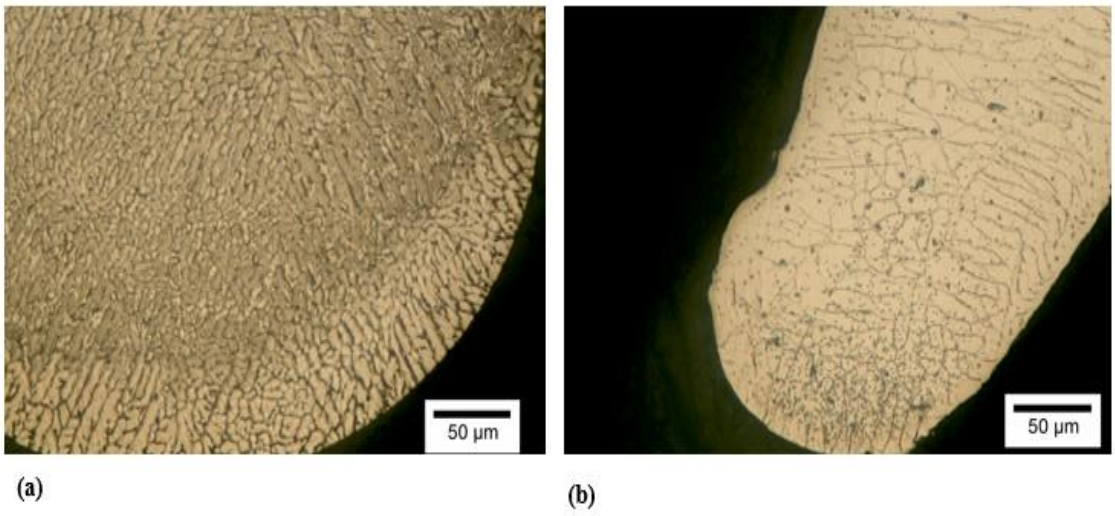

Figure 3.6: a) Micrograph of Al-4.5wt%Cu at the tip of the solidified alloy b) Micrograph of Al-1wt%Cr at the tip of the solidified alloy.

Figure 3.7 depicts the result from the experiment using data acquisition, a K-type thermocouple, and the oscilloscope for fast data acquisition in milliseconds. Figure 3.7a corresponds to the Al-4.5wt% Cu alloy, which has a more excellent temperature range than the Al-Cr alloy. The thermocouple successfully captured the solidification temperature of molten alloy from THC 1 to THC 4, respectively. THC 1 captured a temperature of around 660ºC, which is equivalent to the melting temperature of Al and approximately liquidous temperature of Al-4.5wt%Cu. However, THC 1 could not capture the thermal arrest, and the nucleation of other phases is unclear. Despite other THCs following the predicted pattern from THC 2 to THC 4, the temperatures captured are irrelevant because they are all lower than the solidus temperature of the alloy. This result suggests that the sensitivity or calibration of the THC may be problematic. Also, the design of the experiment may be faulty as the mold cavity is tiny, and the THC is not insulated before inserting into the copper mold. Figure 3.7b depicts the Al-1wt%Cr alloy, which exhibits the same behavior as the previous result, which is irrelevant as it is far from the transition temperatures. THC 1 measured 584ºC temperature, which is close to the solidus temperature of the alloy, while the remaining THC measured temperatures below the solidus temperatures of the alloy. Figure 3.8 shows the microstructure of the Al-4.5wt%Cu and Al-1wt%Cr. The micrograph shows a similar result to Figure 3.6 using the FBGs to capture solidification temperature. It is suspected that the copper mold design does not allow the molten alloy to reach the bottom of the mold before complete solidification.

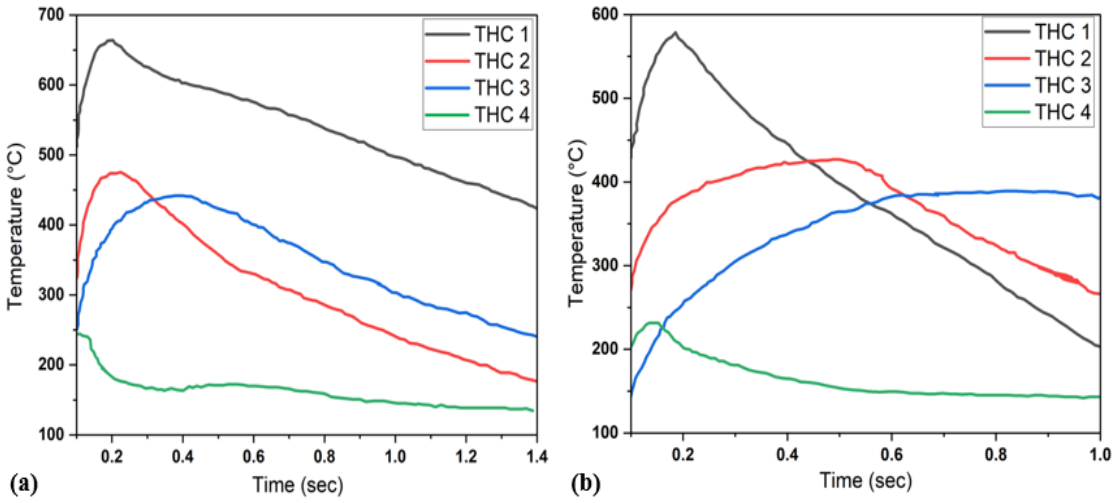

Figure 3.7: a) Temperature vs. time graph for Al-4.5wt%Cu b) Temperature vs. time graph for Al-1wt%Cr.

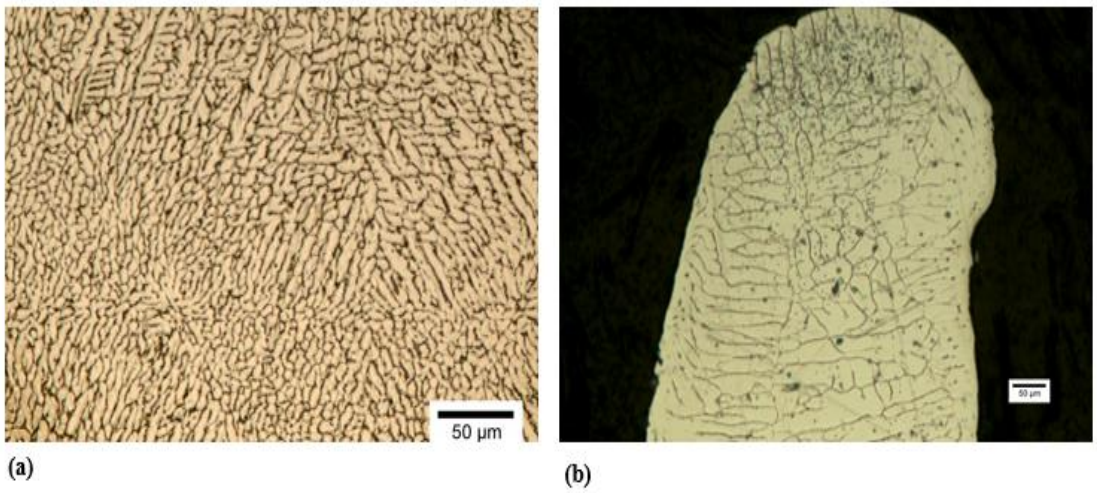

Figure 3.8: a) Micrograph of Al-4.5wt%Cu at the tip of the solidified alloy b) Micrograph of Al-1wt%Cr at the tip of the solidified alloy.

3.3. CONCLUSION

A wedged copper mold solidified Al-Cu and Al-Cr alloys to achieve different cooling rates at other positions. The solidification temperatures were measured using the

FBGs and the K-type thermocouple. Each method captured the solidification temperature, but the experiment was inconsistent and inconsequential.

The microstructure obtained suggests that the molten alloy did not come in contact with the mold wall, allowing the solidified alloy to cool quickly. The mold needs to be redesigned, as the cavity is thinner and needs to be enlarged to enhance the flowability of the molten alloy to the bottom of the mold.

4. CONCLUSIONS AND RECOMMENDATIONS

4.1. CONCLUSIONS

- A predictive model for phase selection as a function of undercooling during rapid solidification, which eliminates kinetic parameters, was developed for binary alloys using aluminum alloys as a case study.
- The phase selection of Al-Zr, Al-Cr, Al-Ti, Al-Mn, Al-Sc, Al-Fe, Al-Ta, and Al-Fe-Si as a function of undercooling was calculated. The model shows a good agreement with the experimental study compared to the previous study and the T_0 curve, which is a thermodynamic parameter.
- The model was extended to multi-component alloys such as ternary alloys and used to demonstrate its merit during precipitation strengthening of alloys.
- Copper wedge mold was used to capture different cooling rates at different positions using two methods. Cooling rates were measured using the FBGs and K-type thermocouple. However, the temperatures measured were inconsistent and showed contradictory values. This may be due to the calibration of the FBGs and the K-type thermocouple setup.
- The microstructure of Al-4.5wt%Cu and Al-1wt%Cr poured into a water-cooled wedge copper mold was analyzed. SDAS ranged from 9μm to 23 μm, while the cooling rate was vague.

4.2. RECOMMENDATIONS

The list of my recommendations for future work is as follows:

- Perform experiments to obtain data to validate multi-component alloys such as Ternary alloys.
- The copper mold cavity must be re-designed to enhance molten alloy flowability to the bottom of the mold before solidification.
- FBG sensor gives a much better result. However, the calibration and mounting of FBG sensor inside the mold cavity needs to be adjusted and redesigned to avoid introducing contaminants or inducing error in the result, such as using the appropriate size of the stainless tube for the firmness of the fiber inside the sleeve of the tube, etc.
- Improved experimental procedure regarding the pouring temperature, holding time of aluminum alloy to allow complete dissolving of intermetallic, using a controlled environment such as an argon atmosphere, minimizing oxidation by removing almost all slag before pouring and stirring with a graphite stir rod.

BIBLIOGRAPHY

[1] W. E. Frazier, “Metal additive manufacturing: A review,” *J Mater Eng Perform*, vol. 23, no. 6, pp. 1917–1928, 2014, doi: 10.1007/s11665-014-0958-z.

[2] G. Shao and P. Tsakiropoulos, “Prediction of phase selection in rapid solidification using time dependent nucleation theory,” *Acta Metallurgica Et Materialia*, vol. 42, no. 9, pp. 2937–2942, 1994, doi: 10.1016/0956-7151(94)90391-3.

[3] K. E. Knipling, D. C. Dunand, and D. N. Seidman, “Criteria for developing castable, creep-resistant aluminum-based alloys - A review,” *International Journal of Materials Research*, vol. 97, no. 3, pp. 246–265, 2006.

[4] “Murray1982_Articles about aluminum alloys.pdf.”

[5] M. Asta, V. Ozolins, and C. Woodward, “A first-principles approach to modeling alloy phase equilibria,” *Jom*, vol. 53, no. 9, pp. 16–19, 2001, doi: 10.1007/s11837-001-0062-3.

[6] T. W. Clyne, “Numerical treatment of rapid solidification,” *Metallurgical Transactions B*, vol. 15, no. 2, pp. 369–381, 1984, doi: 10.1007/BF02667341.

[7] D. M. Herlach, “Reports: A Review Journal Non-equilibrium solidification of undercooled metallic melts,” *Materials Science and Engineering*, vol. 12, pp. 177–272, 1994.

[8] E. Clouet, “Modeling of Nucleation Processes Thermodynamic Approach Conditions for Nucleation,” vol. 22, no. Eq 2, pp. 203–219, 2009, [Online]. Available: www.asminternational.org

[9] J. A. Cahill and A. V. Grosse, “Viscosity and self-diffusion of liquid thallium from its melting point to about 1300°K,” *Journal of Physical Chemistry*, vol. 69, no. 2, pp. 518–521, 1965, doi: 10.1021/j100886a026.

[10] “https://materials.springer.com/.”

[11] W. J. Boettinger, S. R. Coriell, and R. F. Sekerka, “Mechanisms of micro segregation-free solidification,” *Materials Science and Engineering*, vol. 65, no. 1, pp. 27–36, 1984, doi: 10.1016/0025-5416(84)90196-4.

[12] T. Ichikawa, Riei; Ohashi, Teruo; Ikeda, “Effects of Cooling Rate and Supercooling Degree on Solidified Structure of Al-Mn, Al-Cr and Al-Zr in Rapid Solidification,” *Transaction of the Japan Institute of Metals*, vol. 12, no. 5, pp. 280–284, 1971.

[13] I. Riei and O. Teruo, “Effects of the third additional elements on rapid cooled cast structures of Al-3∼5% Mn alloys,” *Journal of Japan Institute of Light Metals*, vol. 16, no. 6, pp. 304–311, 1966, doi: 10.2464/jilm.16.304.

[14] M. R. Abul, R. F. Cochrane, and A. M. Mullis, “Microstructural development and mechanical properties of drop tube atomized Al-2.85wt% Fe,” *J Mater Sci Technol*, vol. 104, pp. 41–51, 2022, doi: 10.1016/j.jmst.2021.05.085.

VITA

Azeez Akinbo was born in Sango Ota, Nigeria. He earned his Bachelor of Science in Mechanical Engineering from the Federal University of Agriculture Abeokuta, Nigeria 2015.

After obtaining his bachelor's degree, Azeez worked as a Field service engineer at IHS Towers Corporate in Nigeria. He left after a year and worked as a Power plant engineer at Rite Foods Limited in Nigeria.

He earned his Master of Science in Material Sciences and Engineering from the Missouri University of Science and Technology in July 2024 under the tutelage of Professor Yijia Gu.